Available online at www.sciencedirect.com
ScienceDirect
Journal of Photochemistry and Photobiology A: Chemistry 185 (2007) 115–126
Journal of Photochemistry and Photobiology A:Chemistry
www.elsevier.com/locate/jphotochem

Carrier gas UV laser ablation sensitizers for photopolymerized thin films

Zhigang Chen, Dean C. Webster *

Department of Coatings and Polymeric Materials, Center for Nanoscale Science and Engineering, North Dakota State University, 1735 NDSU Research Park Drive, Fargo, ND 58105, United States

Received 7 March 2006; received in revised form 18 May 2006; accepted 19 May 2006
Available online 7 July 2006

Abstract

Designed carrier gas UV laser ablation sensitizers were synthesized and proved to greatly enhance the UV laser ablation of photopolymerized thin films. Polymers containing dense ester groups are reported to have better laser ablation performance because of the tendency of the ester groups to decompose into gaseous products ("carrier gases") during the ablation process. In order to introduce this mechanism to cationic UV curable coatings for better laser ablation, a series of "carrier gas" sensitizers were synthesized by reacting hydroxyl containing reactive diluents such as oxetane and polyester polyols with monomethyl oxalyl chloride or dimethyl oxalate; the oxalyl group is considered a "carrier gas" generating moiety. Furthermore, a UV absorbing chromophore, naphthalene, is either chemically bound to the oxalyl containing molecules or blended with the synthesized oxalyl containing compounds to produce a synergistic effect. The "carrier gas" sensitizers were added into a typical cationic UV curable formulation to form sensitized coatings, which were then characterized by thermogravimetric analysis, real time FTIR and ablated by a 355 nm laser. The ablation vias were examined using optical profilometry and SEM. Compared to the control, the sensitized coatings were found to have similar thermal decomposition temperatures and higher functional group conversion during photopolymerization. All of the sensitized coatings containing the "carrier gas" sensitizers exhibited better UV laser ablation performance than the control. The combination of naphthalene derivatives and the oxalyl group gave a better ablation result, suggesting a synergistic effect. The chemical combination of the naphthalene and oxalyl group exhibited better ablation sensitization than their blends, suggesting a more efficient intramolecular laser energy utilization process.

Keywords: UV laser ablation; Carrier gas; Designed sensitizer; UV curable coating

1. Introduction

Laser ablation of polymeric materials is receiving more and more attention due to its advantages in many potential applications such as the fabrication of microfluidic devices [1] and microelectronic/optical parts [2], polymer fuel in laser plasma thrusters, etc. [3]. The mechanism of laser ablation involves both pyrolysis (thermal decomposition) and photolysis (photochemical decomposition) of the material [4]. Photolysis is the preferred mechanism in terms of ablation resolution since the involvement of thermal processes can lead to unwanted deviation from the optimum quality of the structure [5]. Cleaner, higher resolution laser ablation is made possible by advances in laser technology and novel material development. The use of an ultrashort pulse laser such as a femtosecond laser provides a much higher ablation resolution due to the minimization of laser induced heat effects [5–7]. On the material side, new photopolymers have been designed and synthesized. For example, polymers containing the triazene group in the backbone have been synthesized. The photosensitive triazene group absorbs the incident laser energy and photochemically decomposes into gaseous N_2, causing the fracture of the polymer backbone; following which, the N_2 generated (called "carrier gas") ejects out of the ablation site with supersonic velocity, carrying away polymer fragments and ablation debris, resulting in a cleaner, higher resolution ablation structure [3,8]. Polyestercarbonates have also been synthesized and ablated by a 308 nm excimer laser. Because of their absorption at the incident laser wavelength and the gaseous photochemical decomposition products of ester group such as CO and CO_2, they were reported to be ablated faster with a higher resolution of the ablated microstructure [2].

Cycloaliphatic epoxide based cationic UV curable coatings are ideal candidates for microelectronic packaging materials due to their advantages such as good electrical properties [9,10]

* Corresponding author. Tel.: +1 701 231 8709; fax: +1 701 231 8439.
E-mail address: dean.webster@ndsu.edu (D.C. Webster).

1010-6030/$ – see front matter © 2006 Elsevier B.V. All rights reserved.
doi:10.1016/j.jphotochem.2006.05.015

Table 1
Synthesis detail for carrier gas sensitizers

Sensitizer	Reactant ratio (mole)	Catalyst/neutralizer	Synthesis route and procedure	Purification	Characterization	Product appearance
OXT-DMO	OXT:DMO = 1:1	A21 (∼10 wt.% of total reactants)	Scheme 1, route A. Charge reactants in a three neck round bottom flask, reaction under 100 °C in xylene for 12 h w/magnetic stirrer, N_2 purge and water condenser	Vacuum (30 mm Hg) ∼65 °C for 4.5 h to remove the residual xylene and DMO	GC-MS	Viscous clear colorless liquid
Na-MOC	2-Na OH:MOC = 1:1.2	TEA (2–3 times the theoretical amount needed to neutralize the HCl generated during the reaction)	Scheme 1, route B. Charge reactants in a 20 ml glass vial w/THF, stir in water bath w/magnetic stirrer for ∼10 min, charge TEA dropwise, then filter product solution using filter paper to remove the HCl-TEA salt.	Heat filtrate solution on hotplate ∼100 °C w/N_2 purge ∼30 min, followed by vacuum (30 mm Hg) 2–3 h at RT to remove the THF & TEA	GC-MS, UV–vis	Deep brown solid
H-MOC	H:MOC = 1:8				FTIR, UV–vis	Light yellow paste
P-MOC-Na	P:MOC:1-Na Cl = 1:5:1				FTIR, UV–vis	Light yellow clear paste
P-MOC	P:MOC = 1:5				FTIR, UV–vis	Light yellow clear paste
P-Na	P:1-Na Cl = 1:1				HPLC, FTIR, UV–vis	Clear paste

and low shrinkage during UV curing [11]. Using a 355 nm laser to ablate through vias in such coatings is one of the steps in a specific microelectronic fabrication process, but few reports can be found on either 355 nm laser ablation of polymers or laser ablation of UV curable materials. Previously in this lab the 355 nm laser ablation performance of cationic UV curable coatings was successfully improved by incorporating ∼1 wt.% of reactive laser ablation sensitizers as an additive [12]. In our subsequent research aiming to further improve the UV laser ablation performance of these coatings, this additive approach was again adopted, because it was shown in our lab that the addition of laser ablation sensitizers did not significantly change the basic coating properties. In this report, we demonstrate the utilization of the "carrier gas" concept to design and synthesize novel UV laser ablation sensitizers, which greatly enhance the UV laser ablation performance of these coating materials.

2. Experimental

2.1. Materials

Cyracure™ UVR 6110 difunctional cycloaliphatic epoxide (3,4-epoxycyclohexylmethyl-3-4-epoxycyclohexane carboxylate, ECC), UVR 6000 oxetane diluent (3-ethyl-3-hydroxymethyl oxetane, OXT) and UVI 6974 photoinitiator (mixed triarylsulfonium hexafluoroantimonate salt in propylene carbonate, PI) were obtained from Dow Chemical Company. AMBERLYST® 21 ion-exchange resin with tertiary amine functionality (A21), THF (HPLC grade), triethylene amine (TEA), 1-naphthol (1-Na-OH), 2-naphthol (2-Na-OH), 9-anthracene methanol (A-OH), dimethyl oxalate (DMO), 1-naphthalene chloride (1-Na Cl) and mono-methyl oxalyl chloride (MOC) were obtained from Aldrich. Hyperbranched polyester polyols H20 (H) and P1000 (P) were obtained from Perstorp Polyols Inc. The polyol P1000 is in liquid form, which is H20 (solid material) diluted with a polyether type polyol, according to Perstorp Polyols Inc. All materials were used as received.

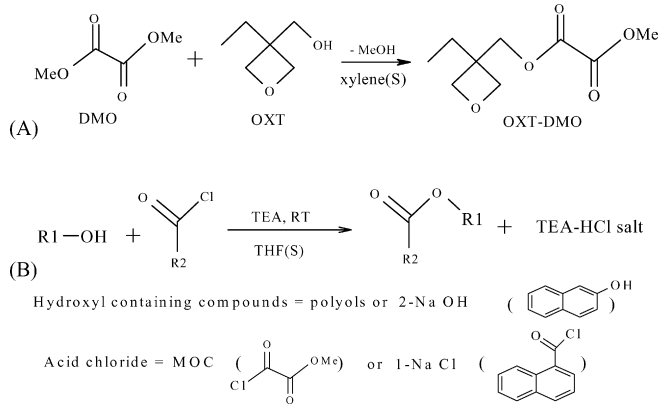

Scheme 1. Synthesis routes of carrier gas sensitizers: (A) synthesis of OXT-DMO by transesterification between OXT and DMO. (B) synthesis involving reaction of hydroxyl group and acid chloride.

Table 2
Nominal structures of synthesized "carrier gas" laser ablation sensitizers

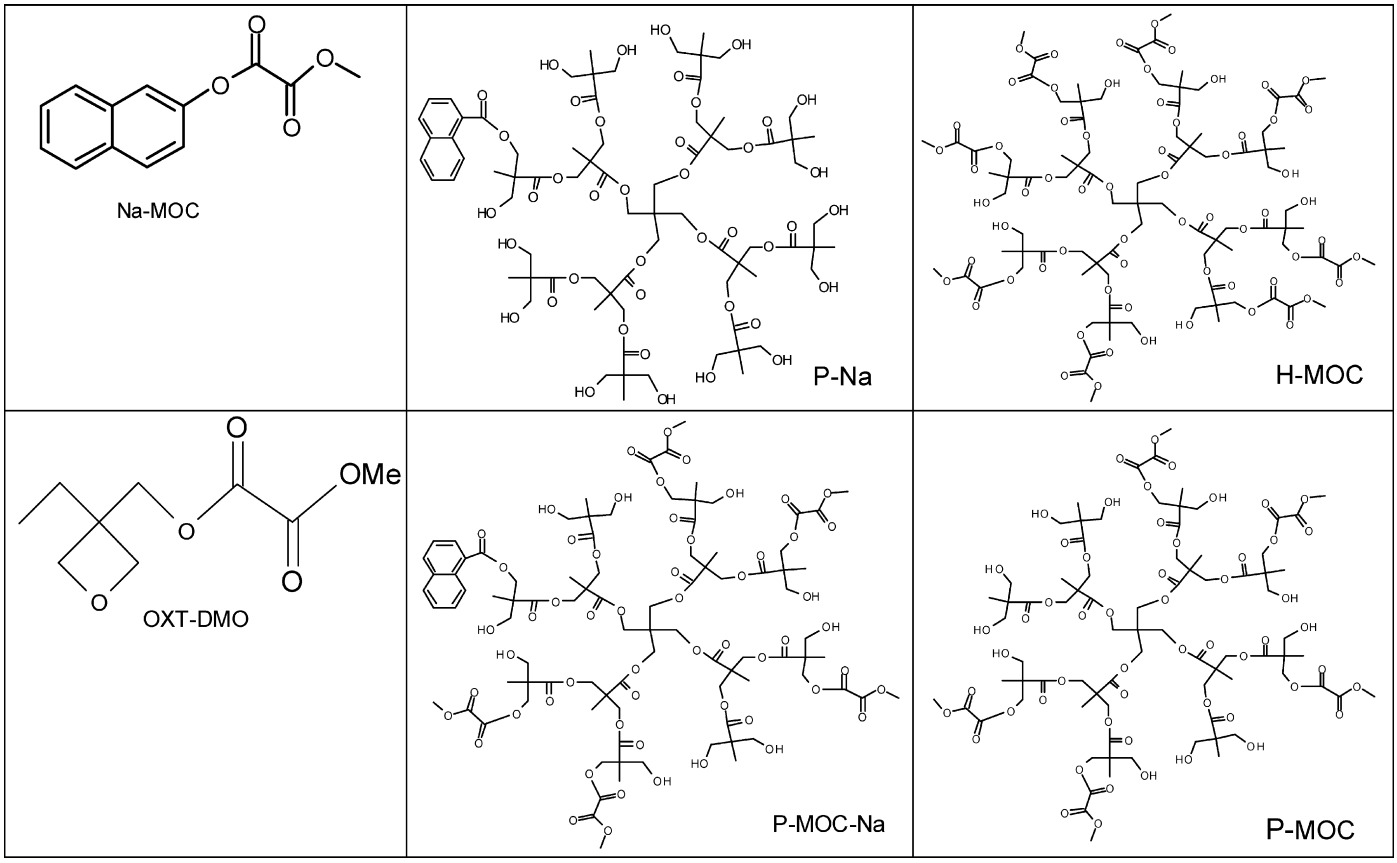

2.2. Synthesis of designed carrier gas sensitizers and sensitized coating formulation

Scheme 1 shows the synthesis routes for designed carrier gas sensitizers and Table 1 shows their synthesis and purification details. Table 2 shows the nominal structures of the synthesized "carrier gas" laser ablation sensitizers.

A series of sensitized coatings were formulated in order to investigate the effect of carrier gas sensitizers. To avoid variation, a masterbase (MB) formulation (also serves as the control formulation) is made and composed of 80 wt.% ECC, 16 wt.% OXT and 4 wt.% PI. This formulation was expected to be ablated with more difficulty due to its high T_g and crosslink density [12]. In using such a formulation it was hoped to differentiate the ablation sensitization performance between the sensitizers. Sensitizers were mixed into the MB formulation under slight heating (~50 °C) to make different sensitized coatings; the compositions are given in Table 3. In Table 3, except for OXT-DMO,

Table 3
Composition of the sensitized coating formulations studied in this work

Formulations	Compositions		
Control	The Master Base (MB) - (80 wt.% ECC, 16 wt.% OXT, 4 wt.% PI		
CG-16	All of the OXT (16 wt.%) in MB are replaced by the reaction product in Scheme 1A		
CG-8	Half of the OXT (8 wt.%) in MB are replaced by the reaction product in Scheme 1A		
CG-(A-OH)	+A-OH	0.0208 g	~0.42 wt.%
Group A			
CG-(1-Na-OH)	+1-Na-OH	0.0144 g	~0.29 wt.%
CG-(Na-MOC)	+Na-MOC	0.023 g	~0.46 wt.%
CG-(H-MOC)	+H-MOC	0.2188 g	~4.4 wt.%
CG-(H-MOC + 1-Na-OH)	+H-MOC and 1-Na-OH	0.2188 + 0.0144 g	~4.7 wt.%
Group B			
CG-(P-MOC)	+P-MOC	0.193 g	~3.9 wt.%
CG-(P-Na)	+P-Na	0.1655 g	~3.3 wt.%
CG-(P-MOC + 1-Na-OH)	+P-MOC and 1-Na-OH	0.193 + 0.0144 g	~4.1 wt.%
CG-(P-MOC-Na)	+P-MOC-Na	0.208 g	~4.2 wt.%

all the other sensitizers were added at the ratio of 0.0001 mol/5 g MB. (If there are two sensitizers added, then each of them was added at the ratio of 0.0001 mol/5 g MB; the theoretical molecular weight of the sensitizer was used for the calculations.)

2.3. Characterization

GC-MS analysis was performed on an HP 6890 gas chromatograph with an HP 5973 mass selective detector utilizing EI (electron ionization) with filament energy of 69.9 keV. The front inlet was in split mode with inlet temperature of 250 °C and pressure 8.24 psi, split ratio was 50:1. Initial GC oven temperature was 70 °C for 2 min, and then the temperature was ramped to 300 °C at a rate of 20 °C/min and was held for 16.5 min. Total run time was 30 min. Separation was achieved on a ZEBRON ZB-35 capillary column operated in a constant flow mode with flow rate of 1.0 ml/min. The average velocity was 36 cm/s. the mass spectrometer was in scan mode with m/z range from 10 to 800. The temperatures for MS source and MS Quad were set at 230 and 150 °C, respectively.

The FTIR and real time FTIR (RTIR) experiments were performed using a Nicolet Magna-IR 850 Spectrometer Series II with detector type DTGS KBr. For the RTIR experiments, a UV optic fiber is mounted in a sample chamber in which the humidity is kept around 20% by Drierite®. The light source was a LESCO Super Spot MK II 100 W DC mercury vapor short-arc lamp. This setup directly monitors the functional group conversion as the photo polymerization reaction proceeds. Coating samples were spin coated onto a KBr plate at 3000 rpm for about 15 s, which were then exposed to UV light for 60 s. Scans were taken over a 120 s period at 2 scans/s. The UV intensity was adjusted to ~3.6 mW/cm^2 and the experiment was performed in air. The oxirane conversion of ECC was monitored at 789 cm^{-1} and the oxetane conversion of EHMO was monitored at 976–977 cm^{-1}. The average conversion at 120 s is presented. The average standard deviation of this experiment is ±2%.

Cured coating films were prepared by casting the liquid sample onto an aluminum panel (Q panel) with a Gardco 70# wire drawdown bar, followed by UV curing for 60 s in air using a Dymax light source with a 200 EC silver lamp (UV-A, 365 nm). The intensity was ~35 mW/cm^2 measured by a NIST Traceable Radiometer, International Light model IL1400A. Cured coating films are ~80–100 μm thick measured by Micromaster® micrometer. The purpose of preparing such an unusually thick film is to monitor the laser ablation progress inside the coating film as the pulses increases. Free coating films were peeled off from aluminum panel using a razor blade for TGA analysis and laser ablation experiments.

UV laser ablation on cured coating films was done using a Continuum Surelite II Nd:YAG laser in a single shot mode. The laser beam passes through a Pellin-Brocca light prism into a Newport Model 935-5 attenuator, and then is focused on the sample surface using a Newport U-27X objective lens. Free coating films were taped on ZAP-IT laser calibration panel and mounted on a 3D sample mount, the distance between the laser output and the sample film was 80 cm. The laser wavelength is 355 nm with a beam spot size of approximately 40 μm. The pulse energy was adjusted to a lower value of ~0.93 mJ (measured using Molectron J9LP pyroelectric detector before lens) in order to better differentiate the sensitized samples. Each sample film was ablated under the same conditions and the ablation experiment was performed in air. The ambient temperature of the laboratory was approximately 25 °C. Two rows of vias were ablated on each sample film as shown in Fig. 1; vias in each row were ablated by laser pulses of 1, 2, 4, 8, 16 and 32 respectively, with the second row as a repetition of the first one. The via depth and volume data are based on the average value of these two identically ablated vias.

Fig. 1. Ablated via array on coating film in UV laser ablation experiments.

Wyko NT3300 Optical Profilometry from VEECO was used to obtain profile data of ablated vias. Vertical scanning interferometry (VSI) mode and a magnification of 50 × 0.5 were used. Back scan length was set at 15 μm, scan length was varied from 100 to 150 μm as pulses increases. Vision 32 for NT-2000 software, Version 2.303 was used to process the dimension data for ablated vias. Scanning electron microscopy (SEM) images were obtained using a JEOL JSM-6300 Scanning Electron Microscope. Samples were mounted using carbon sticky tabs on aluminum mounts and coated with gold/palladium using a Balzers SCD 030 sputter coater.

UV–vis spectra were obtained on a Varian Cary 5000 UV–vis–NIR spectrophotometer operating in absorption mode. The scanning rate was 600 nm/min and scanning range was 200–600 nm. The compounds were dissolved in acetonitrile for the UV–vis experiments. Thermogravimetric analysis (TGA) was performed using a TA Instruments TGA Q500 under nitrogen purging, the temperature was ramped from 25 to 650 °C at a ramping rate of 10 °C/min, the inflection point of the major degradation transition is presented as T_d.

3. Results and discussion

3.1. Synthesis and effect of OXT-DMO—the first trial

The use of "carrier gas" laser ablation sensitizers to improve the UV laser ablation performance of photopolymerized thin film materials is a novel approach. In order to realize this concept and obtain a "carrier gas" laser ablation sensitizer, rational molecular design followed by tailored synthesis is indispensable. In the design stage for these novel sensitizers, two key aspects were taken into consideration. The first was the choice of the "carrier gas" generating functional group in the sensitizer molecule. Though nitrogen containing functional groups such as triazene have been reported to be effective in generating carrier gas (N_2) upon photolysis [3,8], the basicity of such groups may inhibit the cationic photopolymerization of the oxirane and oxetane [13]. The oxalyl group was then chosen over the ester group as the best candidate for the "carrier gas" generating functional group due to its dense ester structure and the tendency to decompose into small molecule gases such as CO and CO_2. The

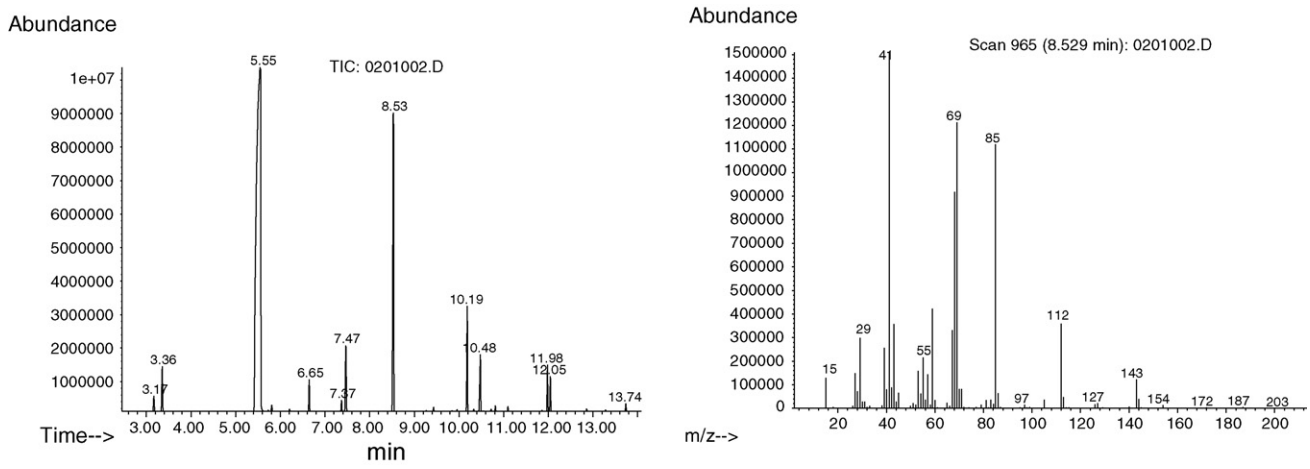

Fig. 2. GC chromatogram (left) and MS spectrum (right) for the synthesis product of OXT-DMO.

second consideration was that it seems advantageous to chemically attach the oxalyl group to the monomers in the coating composition, so that the resulting sensitizer will have better compatibility with the coating matrix and be uniformly distributed throughout the material. Based on these thoughts, synthesis was carried out to attach the oxalyl group to the hydroxyl oxetane monomer through transesterification as shown in Scheme 1A. The reaction product was named OXT-DMO.

The synthesis and purification of OXT-DMO is a time consuming process. The reaction product was dried in a vacuum oven and then characterized by GC-MS; the result is shown in Fig. 2. In the GC chromatogram, the 3 min peaks are residual DMO and xylene, the 5.5 min peak is unreacted OXT, 8.5 and 10 min peaks are identified as the desired mono transesterification product: OXT-DMO. The other peaks are by-products. The purified product contains over 50% of unreacted OXT and only about 30% of the desired product, OXT-DMO. In the MS spectrum of 8.5 and 10 min peaks, the molecular ion of OXT-DMO with $m/z = 202/203$ appears at the right end. The fragmentation of OXT-DMO starting from the DMO side is indicated by the lower m/z peaks. For example, peak $m/z = 187$ indicates the loss of $–CH_3$, peak $m/z = 171/172$ indicates the loss of $–OCH_3$, and peak $m/z = 143$ indicates the loss of $–COOCH_3$. Two conclusions are apparent from the GC-MS results: (1) the route for the synthesis of OXT-DMO results in a low product yield; (2) the oxalyl group will readily decompose and release the desired gaseous products upon high energy input.

Although the content of OXT-DMO in the reaction product (30% OXT-DMO, >50% OXT) is low, it was incorporated into formulations (CG-16 and CG-8) for an initial assessment of the three most important coating properties: UV curing behavior, thermal stability and laser ablation performance, as compared to the control samples. The other minor impurities such as DMO were not expected to have a major impact on the coating properties. The RTIR and TGA results for coating sample CG-16, CG-8 and two control samples are presented in Table 4. No major change was observed in the UV curing behavior and thermal stability of coatings after substituting the OXT with OXT-DMO.

Table 4
RTIR and TGA result of coatings with OXT-DMO in comparison with the control and A-OH sensitized coatings

Formulations	RTIR 120 s conversion (%)		T_d (°C)
	Epoxide	Oxetane	
Control	43	66	394
CG-16 (contains ~5 wt.% OXT-DMO)	48	62	393
CG-8 (contains ~2.4 wt.% OXT-DMO)	42	63	388
CG-(A-OH)	45	63	393

The laser ablation data of these samples is given in Table 5, where letter "N" denotes no ablation, "T" denotes that a through hole is ablated in the coating film, "B" stands for the scenario that bulk coating material still exists in the center of the hole while the surrounding material has been removed (illustrated in Fig. 3A), and letter "C" denotes that a relatively clean hole is ablated (illustrated in Fig. 3B). Here the ablation scenario graded by letter "B" is considered a less efficient removal of material by laser ablation than the scenario graded by letter "C". The numbers in Table 5 are the deepest via depth (in μm) data obtained from the "filtered histogram" analysis. The filtered histogram (included in Vision 32 software) is a line graph representing the number of data points at each surface depth of the entire mea-

Table 5
Deepest ablated via depth (μm) for OXT-DMO containing coatings in comparison with the control and A-OH sensitized samples

Laser pulses	Control	CG-16	CG-8	CG-(A-OH)
1	N	62.5, C	N	53.5, B
2	N	101.0, T	N	54.3, B
4	N		N	56.8, B
8	N		N	75.0, B
16	35.0, B		74.4, B	114.0, T

N: no ablation; B: bulk material exists in the center of the hole as shown in Fig. 3A; C: a clean hole is ablated as in shown in Fig. 3B; T: a through hole ablated in the coating film.

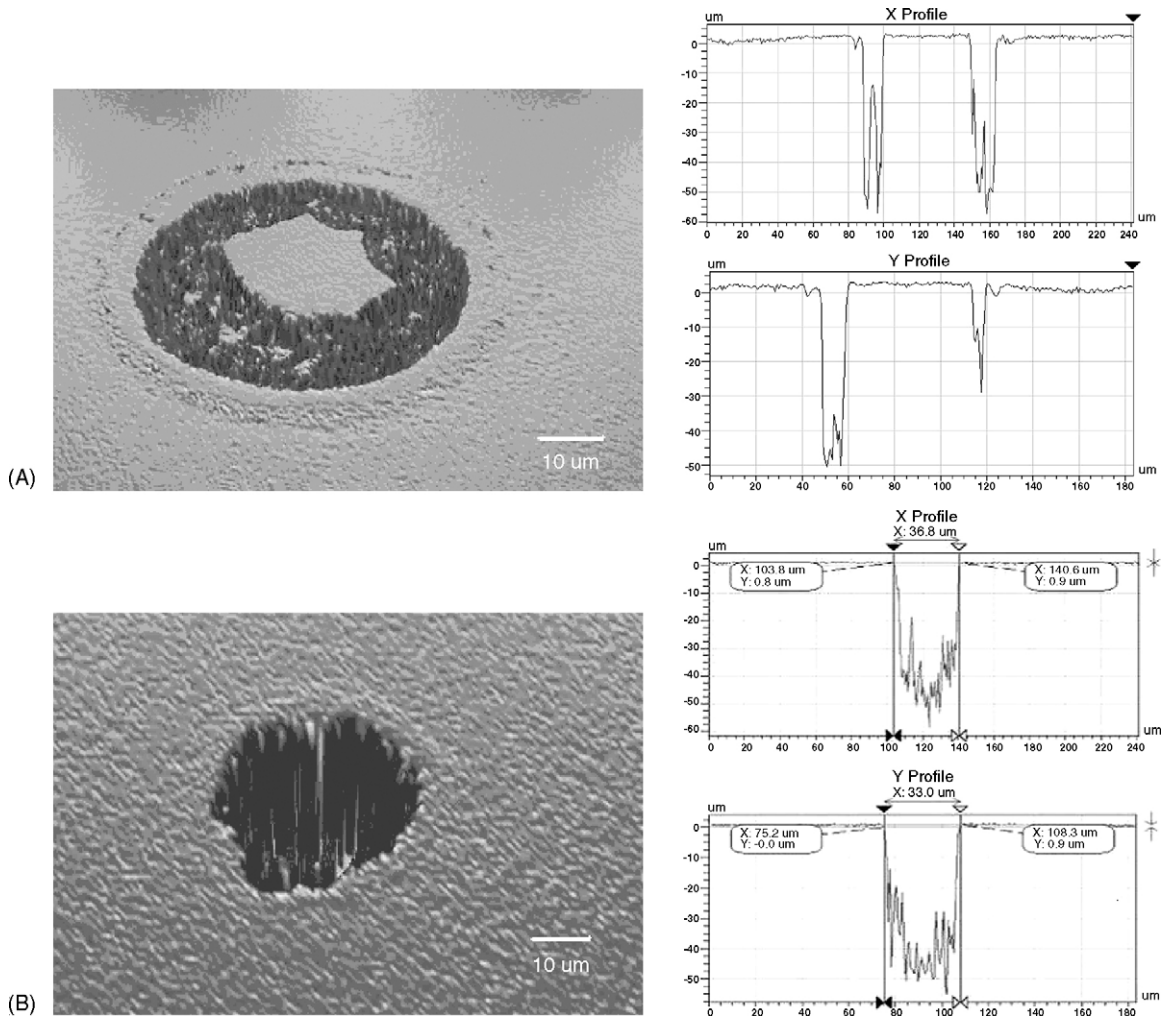

Fig. 3. (A) 3D and cross-section view of holes with materials remain in the center. (B) 3D and cross-section view for a "cleaner" hole. Diameter of the via can be found from the cross-section view on the right.

sured area for the ablated vias; this graph is used to find the deepest depth of the ablated vias. The diameter of the ablated vias is around 30–50 μm.

From Table 5 it is apparent that the coating CG-16 has much better ablation than the other samples, especially the control and CG-8, for which the ablation starts only at 16 pulses. As to the coating CG-(A-OH), with the addition of anthracene methanol that absorbs at around 355 nm, its ablation starts as early as CG-16, but the removal of material is less complete. As laser pulses increase, the ablation depth for coating CG-(A-OH) increases and the central material bulk decreases in size due to laser ablation, but only at 16 pulses does the central bulk material disappear. These preliminary results suggest the efficacy of the "carrier gas" generating oxalyl group; however, it appears that a relatively large amount of OXT-DMO is needed to achieve good ablation. As to the difference observed between coating CG-(A-OH) and CG-16, the explanation is that for materials doped by polyaromatic compounds such as the anthracene methanol, ablation is based on a photothermal mechanism—the material is heated up by the thermal energy converted from the laser photon energy absorbed by those absorbent chromophores [14,15]. On the other hand, although the ablation of OXT-DMO sensitized samples is also probably based on the photothermal mechanism since the OXT-DMO and the coating material has no absorption at 355 nm, the laser energy utilization may follow a different route. It was reported that during laser ablation, unlike pyrolysis, where the sample temperature is raised in a relatively slow fashion and the decomposition of the sample is characterized by cleaving the weakest bond, the ablative thermal decomposition will raise the sample temperature almost instantaneously to a value that is high enough to activate most of the possible decomposition paths simultaneously [16]. Therefore, for the ablation of OXT-DMO containing films, due to the decomposition tendency of the oxalyl group, the OXT-DMO may easily and simultaneously decompose into several gaseous fragments during the laser ablation process, consequently the released "carrier gases" such as CO and CO_2 can effectively eject more film material from the ablation site to create a cleaner hole.

3.2. Design, synthesis and characterization of "carrier gas" laser ablation sensitizers

While the initial UV laser ablation result after incorporating OXT-DMO is encouraging, the synthesis and purification

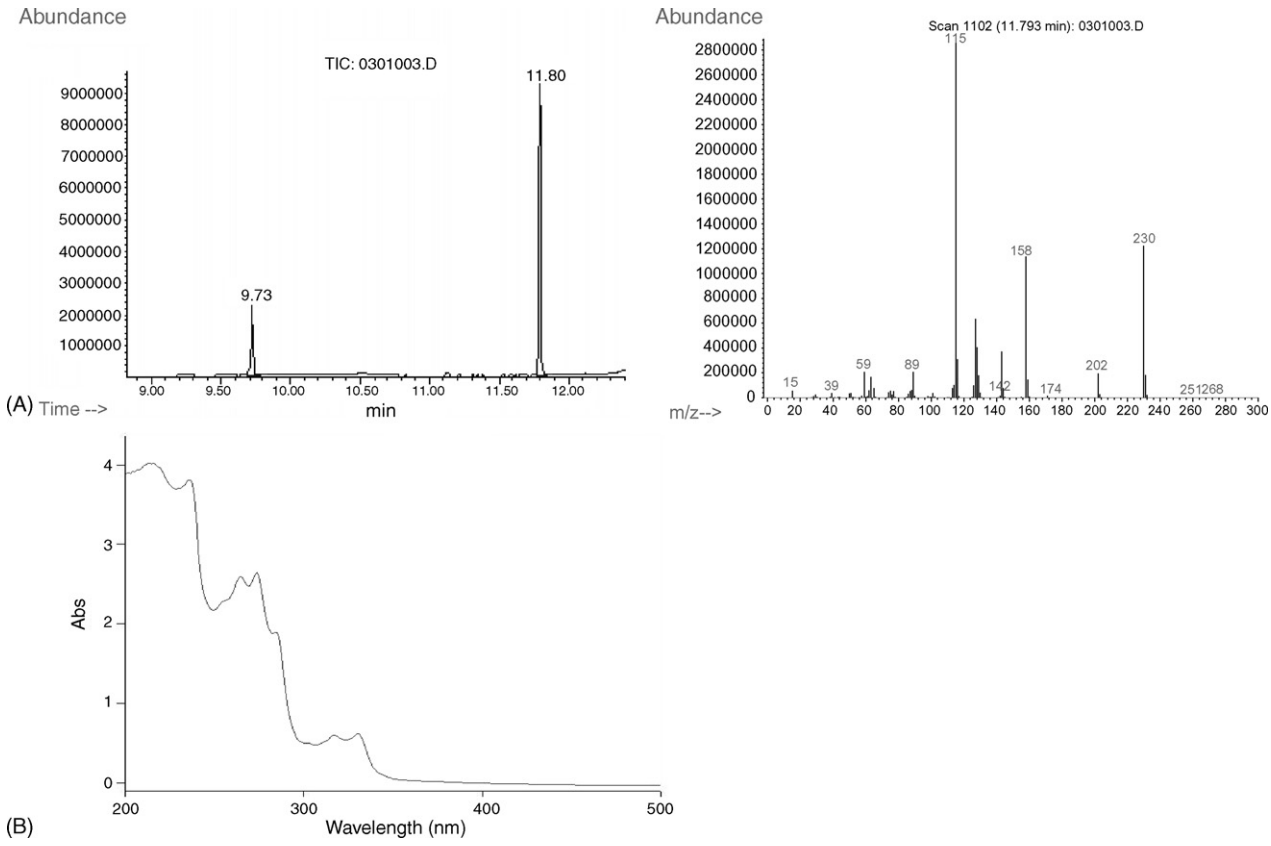

Fig. 4. (A) GC chromatogram (left) and MS spectrum (right) of Na-MOC. (B) UV–vis spectrum of Na-MOC.

of OXT-DMO is lengthy with a low yield. On the other hand, it was thought that better laser ablation can be achieved with a sensitizer molecule having a 355 nm UV absorbing chromophore such as anthracene or naphthalene and the oxalyl groups chemically linked together. In this way the laser energy absorbed by the chromophore can be efficiently transferred to the oxalyl groups intramolecularly, and consequently induce the decomposition of oxalyl groups into carrier gases either thermally or photochemically. It was also expected that if these two functional groups are linked closely enough, they will synergistically respond to the incident laser energy and decompose photochemically, thus minimizing energy loss during energy transfer process. Thus, subsequent synthesis efforts were focused on the design of sensitizer molecules embodying the above considerations. Since the synthesis trials using transesterification and esterification routes were not promising, the hydroxyl–acid chloride reaction shown in Scheme 1B was chosen as an alternative. With this chemistry, a series of "carrier gas" laser ablation sensitizers with UV absorbing chromophores and oxalyl groups bound to one molecule were systematically designed and synthesized. Table 1 provides the synthesis and purification details for these sensitizers and their nominal structures are shown in Table 2. Their characterization information is given below.

The theoretical molecular weight of Na-MOC is 230.22; its GC-MS analysis and UV–vis spectrum are shown in Fig. 4A and B, respectively. In the GC chromatogram (left), the 9.73 min peak is unreacted 2-Na-OH as confirmed by a GC-MS experiment with the pure 2-Na-OH sample; the 11.80 min peak is Na-MOC. The MS spectrum of Na-MOC (right) shows its molecular ion peak $m/z = 230$. The product contains >80% Na-MOC. The UV–vis spectrum of Na-MOC has more extended absorption (up to 400 nm) than that of naphthalene, which is the result of the linkage of two conjugated groups, the naphthalene and the oxalyl group. Consequently, Na-MOC not only has naphthalene and oxalyl group directly bound to each other in one sensitizer molecule as desired, it also has the extra advantage of extended UV absorption covering the incident laser wavelength at 355 nm. The P-Na was synthesized in previous work in this lab, which purity is 95.5% as indicated by HPLC peak area integration [17].

For the synthesis of H-MOC, P-MOC and P-MOC-Na, the concept was to attach multiple oxalyl groups to one polyol molecule, so that more gaseous product will be generated upon the decomposition of the sensitizer molecule. The hyperbranched polyester type polyols H and P proved to be the ideal starting materials for further chemical "decoration" due to their multiple hydroxyl functional groups (16 and 15 theoretical hydroxyl groups per molecule for polyols H and P, respectively). The H-MOC, P-MOC and P-MOC-Na were characterized using FTIR and UV–vis as shown in Figs. 5 and 6. Compared to the starting polyols P and H, a distinct feature in the FTIR spectra of these products is the decrement of the hydroxyl peak at 3300–3400 cm^{-1} and the increment of carbonyl peak at ~1750 cm^{-1}, indicating the attachment of oxalyl group by react-

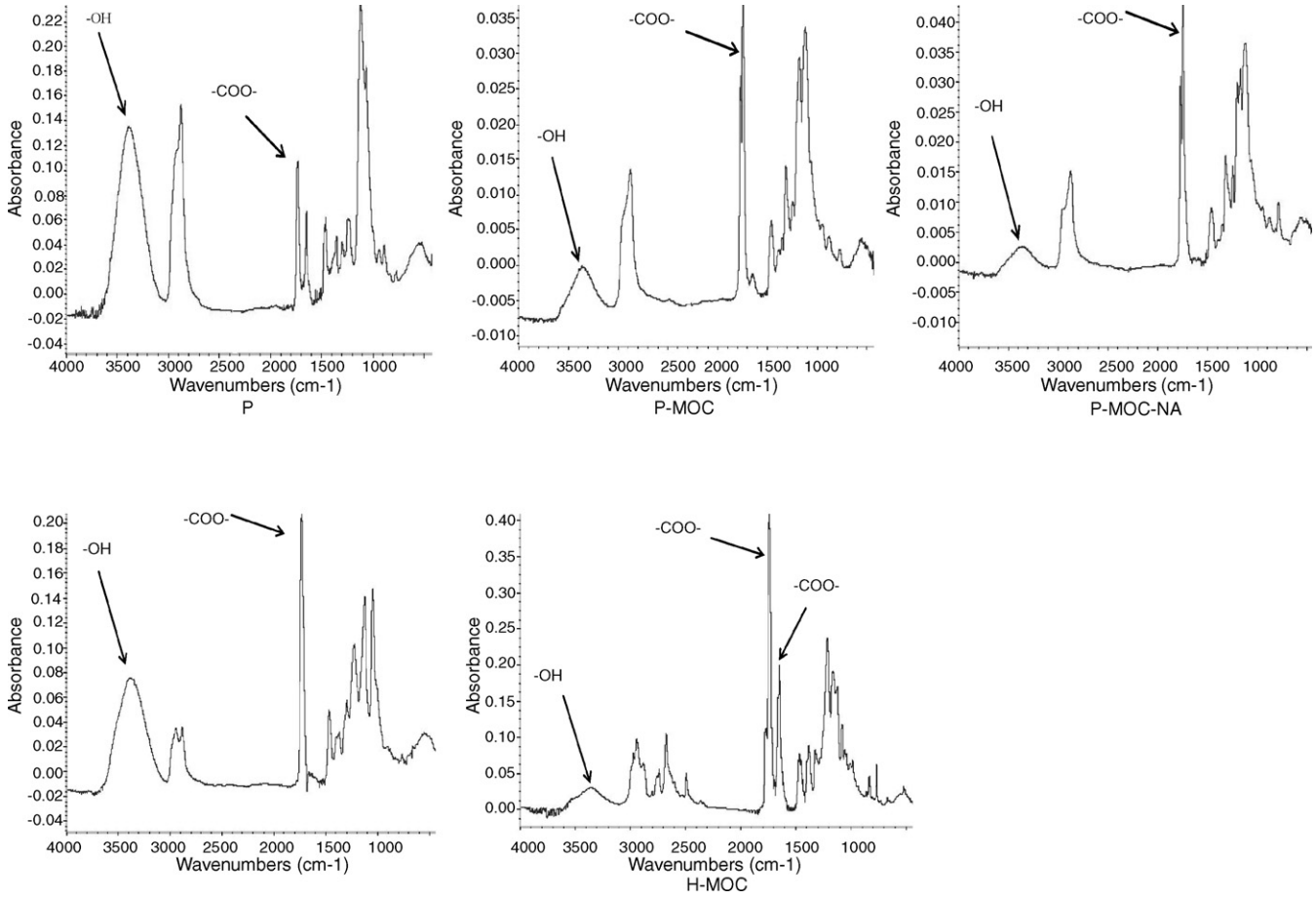

Fig. 5. FTIR spectra of polyol H and P based "carrier gas" sensitizers.

ing some of the polyol hydroxyl groups. The UV–vis spectra of these synthesis products (shown in Fig. 6) are all different from the starting material H (or P), which has only a weak absorption around 250 nm. Also, it is noticed that after the attachment of naphthalene, as in the case of P-MOC-Na, the UV–vis absorption of the sensitizer molecule is extended to around 350 nm.

3.3. Effect of "carrier gas" laser ablation sensitizers in photopolymerized films

The designed "carrier gas" sensitizers were added into the masterbase formulation to make sensitized coatings. The amount of addition is ∼3–5 wt.% for H and P based sensitizers and

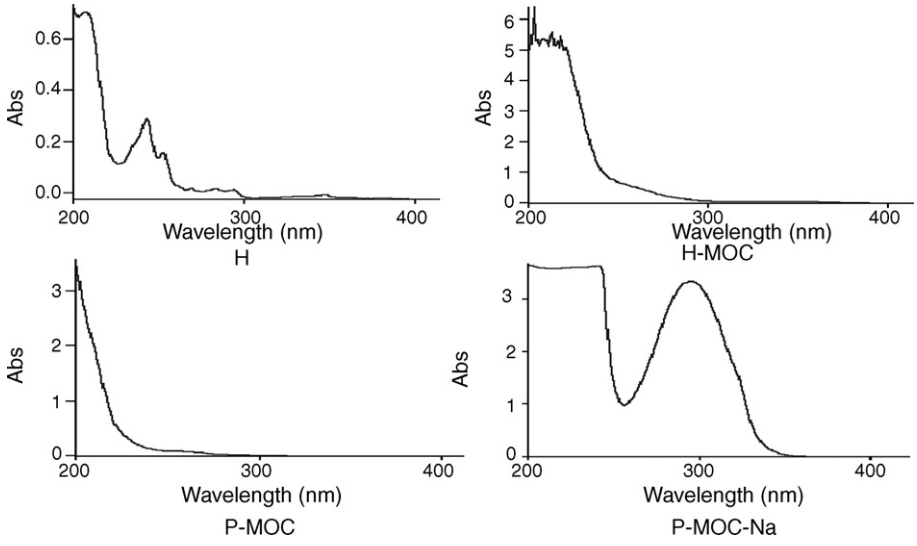

Fig. 6. UV–vis absorption spectra of polyol H and P based "carrier gas" sensitizers.

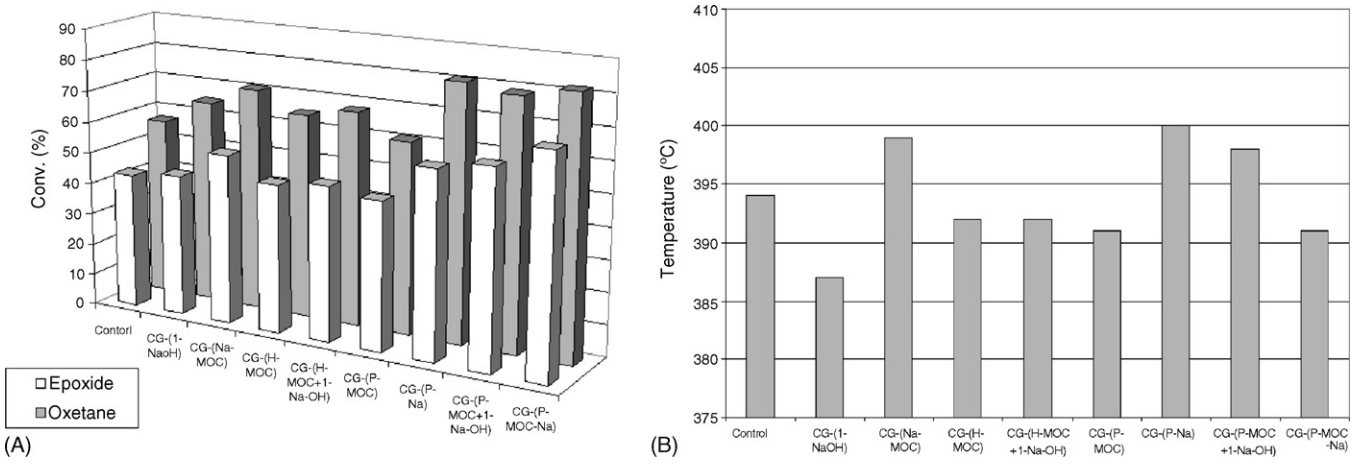

Fig. 7. (A) Reactive functional group conversion (%) at 120 s for sensitized coatings in RTIR experiment. (B) T_ds of sensitized coatings.

<0.5 wt.% for the others. For better comparison, these formulations were divided into groups A and B as shown in Table 3. Group A includes coatings with H derivatized sensitizers and other formulations, group B includes all coatings containing P derivatized sensitizers. These coatings together with the control sample were then characterized by RTIR and TGA followed by UV laser ablation to examine the effect of the added sensitizers.

The RTIR experiment results are shown in Fig. 7A, where it can be seen that none of the sensitized coatings exhibit deterred UV curing compared to the control sample. A slight increase in reactive functional group conversion is observed after the addition of H-MOC or P-MOC while an appreciable increase in reactive functional group conversion after the addition of naphthalene derivatives is noticed, which is attributed to their photosensitizing effect [18–21]. The extended UV absorption may account for the extraordinary photosensitizing effect of Na-MOC. It should also be noticed that when the naphthalene is chemically bound to a polyol species, the resultant sensitizer provides a much more pronounced photosensitization effect as can be seen in the case of P-Na and P-MOC-Na. This phenomenon can be explained by the Intramolecular Hydrogen Abstraction Photosensitization mechanism as proposed previously [17], while the even better photosensitization effect of P-MOC-Na than P-Na may be due to the strengthened UV absorption of P-MOC-Na molecule contributed by the conjugated oxalyl groups. As to the thermal stability, TGA results in Fig. 7B show no significant change of T_d for sensitized samples as compared to control sample – all of the T_ds vary around 390 °C within a 15 °C range.

The variation in chemistry and molecular structure of the sensitizer molecules resulted in a significant difference in the UV laser ablation performance of the sensitized coatings. Table 6 summarizes the via's deepest depth for groups A and B coatings. The volume data of some better ablated vias in groups A and B were also obtained using the "multiple region analysis" tool in the Vision 32 software and is presented in Fig. 8; this data is considered to be a better representation of how well the via is ablated.

From the ablation data, it is first noticed that the UV laser ablation performance of all sensitized samples is much better than the control sample for which the ablation does not start until 16 pulses as shown in Table 5, while all the sensitized samples begin

Table 6
Deepest ablated via depth (μm) for groups A and B sensitized coatings.

Pulses/sensitized coatings	CG-(1-Na-OH)	CG-(Na-MOC)	CG-(H-MOC)	CG-(H-MOC+1-Na-OH)
Group A				
1	B	55.1, B	44.9, B	55.6, C
2	55.9, B	76.3, C	54.3, B	56.3, C
4	39.5, B	113.5, T	68.2, C	79.2, C
8	63.0, B		105.5, T	104.0, T
16	94.0, T			

	CG-(P-Na)	CG-(P-MOC-Na)	CG-(P-MOC)	CG-(P-MOC+1-Na-OH)
Group B				
1	61.7, B	71.3, C	23.3, B	72.4, C
2	59.0, B	72.3, C	24.0, B	99.5, T
4	69.6, C	85.1, C	95.0, B	
8	124.0, T	85.3, C	103.0, T	
16		113, C		

N: no ablation; B: bulk material exists in the center of the hole as shown in Fig. 3A; C: clean hole is ablated as in shown in Fig. 2B; T: through hole ablated in the coating film.

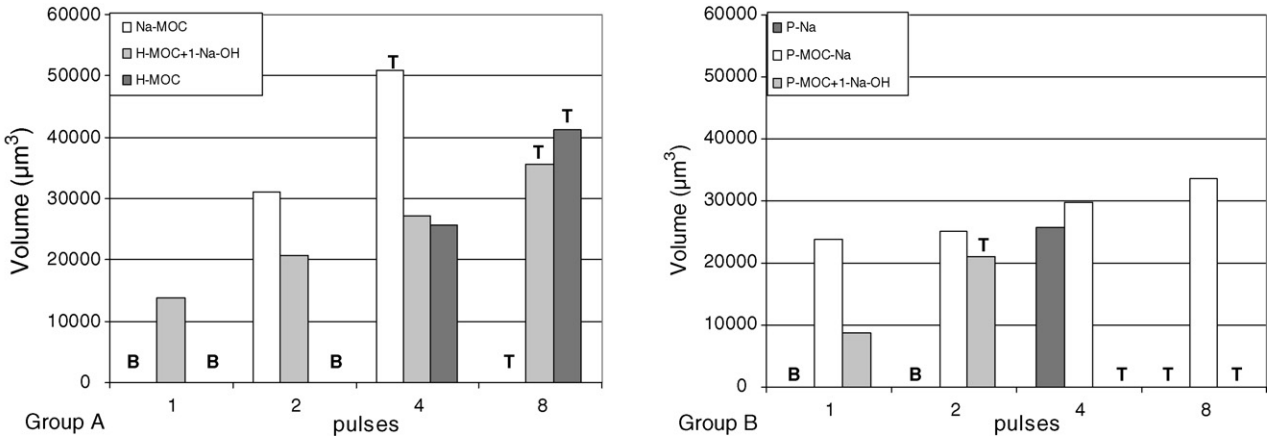

Fig. 8. Via volume data of some sensitized coatings. B, bulk material exists in the center of the hole as shown in Fig. 3A; T, a through hole ablated in the coating film.

to be ablated within two pulses. For group A coatings, in terms of laser ablation performance, they can be ranked in the following order (from better to worse): CG-(Na-MOC) > CG-(H-MOC + 1-Na-OH) > CG-(H-MOC) > CG-(1-Na-OH). The addition of the naphthalene derivative alone (CG-(1-Na-OH)) gives the least efficient removal of material at the ablation site. When the carrier gas generation moiety is added (CG-(H-MOC)), a cleaner and deeper via than CG-(1-Na-OH) is achieved at 4 pulses. When both naphthalene and oxalyl groups are present in the formulation, as in the case of CG-(Na-MOC) and CG-(H-MOC + 1-Na-OH), a synergistic effect that gives much better laser ablation can be observed: both formulations achieved a clean, deep hole within 2 pulses. A scenario can be envisioned to explain the better ablation of these two samples: the more "vulnerable" oxalyl functional group utilizes the energy absorbed by the laser energy absorber – naphthalene – either thermally or photochemically, and decomposes into carrier gases which then create a larger and cleaner via. Furthermore, by comparing the ablation data for coating CG-(Na-MOC) and CG-(H-MOC + 1-Na-OH), it is noticed that the ablated holes of CG-(Na-MOC) are deeper and larger than that of CG-(H-MOC + 1-Na-OH), so it seems the synergistic effect is more effective when the two functional groups – the naphthalene and the oxalyl group – are chemically bound to each other than when they are just physically blended. The explanation for this is that for sensitizer Na-MOC, since its naphthalene and oxalyl group are directly linked to each other, it has a more extended UV absorption than 1-Na-OH as a result of conjugation. It is also very possible that the oxalyl group can directly utilize the absorbed laser energy by the whole Na-MOC molecule to decompose into carrier gases, so energy loss during energy transfer is minimized. The decomposition of Na-MOC is most probably a photochemical process. As to the physical blend of H-MOC and 1-Na-OH, a plausible energy utilization route is as follows: the absorbed laser photon energy is converted to thermal energy by naphthalene first, then transfers though the coating material to the H-MOC molecule and thermally decomposes it. This process is less efficient considering the loss during energy transportation. The other difference between sample CG-(Na-MOC) and CG-(H-MOC + 1-Na-OH) is that the sample CG-(H-MOC + 1-Na-OH) contains seven times more oxalyl groups than CG-(Na-MOC). Also the Polyol H in H-MOC brings in additional ester groups. The existence of a large amount of potential carrier gas generation moieties will definitely compensate for its less efficient energy utilization process during laser ablation of the coating, which may account for the difference observed at the first ablation pulse for these two formulations.

Sensitized coating samples in group B are all Polyol P based derivatives. Their ablation performance can be ranked as: CG-(P-MOC-Na) > CG-(P-MOC + 1-Na-OH) > CG-(P-Na) > CG-(P-MOC). The effect of P-Na is better than 1-Na-OH and P-MOC, which may be due to the fact that naphthalene is attached to a polyester polyol, so it is easier for the ester groups to intramolecularly utilize the absorbed laser energy by naphthalene to decompose and generate carrier gases, but such utilization may not be photochemical. The better laser ablation performance of CG-(P-MOC-Na) and CG-(P-MOC + 1-Na-OH) was expected because of the decomposition tendency of the oxalyl group and its synergistic effect with naphthalene as discussed earlier. Ablated vias of CG-(P-MOC-Na) are larger in volume than those of CG-(P-MOC + 1-Na-OH), this may be due to the more efficient intramolecular energy utilization process.

When comparing the best samples from groups A and B, it is found that the via volume for CG-(Na-MOC) is larger than that of CG-(P-MOC-Na), even though both are considered to have an intramolecular synergistic effect. However, by envisioning the theoretical structure of P-MOC-Na as shown in Table 2, this observation can be accounted for. The hyperbranched core of P-MOC-Na is Polyol H, which is the main ingredient of Polyol P. It has 8 branches with 16 hydroxyl groups on one molecule. For the synthesis of P-MOC-Na, the reactant ratio is Polyol P:MOC:1-Na Cl = 1:5:1, so statistically naphthalene is still not that close to the oxalyl groups, subsequently the energy transfer will not be as facile and efficient as in Na-MOC. It is expected that if more oxalyl groups are attached, the intramolecular synergistic effect will be more pronounced. But in spite of this, it is obvious that the combination of the carrier gas generation group and UV absorber results in much better laser ablation.

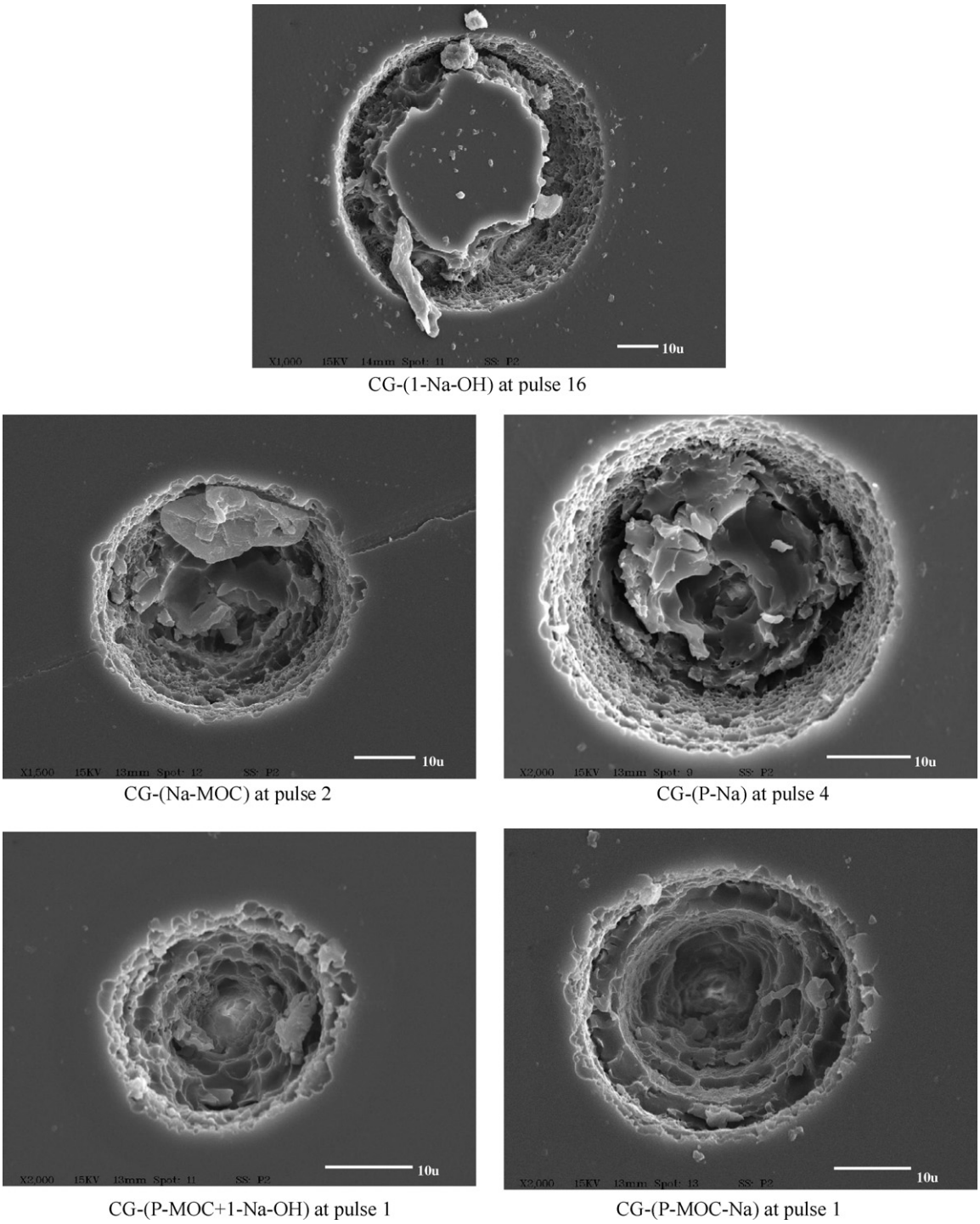

Fig. 9. SEM images of some UV laser ablated vias.

SEM images were taken for some of the ablated vias as shown in Fig. 9, which further corroborates the results obtained from profilometry. For sample CG-(1-Na-OH), even at 16 pulses, the material is not completely removed at the ablation site and ablation debris can be seen deposited at and around the ablation site. As for the sample CG-(Na-MOC) and CG-(P-Na), the ablation of CG-(Na-MOC) at 2 pulses gives cleaner material removal inside the ablated via than the ablation of sample CG-(P-Na) at 4 pulses. A more amazing scenario is observed for sample CG-(P-MOC + 1-Na-OH) and CG-(P-MOC-Na). Even at 1 pulse, the ablation of both samples gives a much cleaner ablated via than all the other samples shown in Fig. 9. These SEM images provide direct visual evidence that further confirm the effect of the carrier gas sensitizers and the synergistic effect during laser ablation.

The current high resolution UV laser ablative microstructuring of polymeric materials is limited to those materials that have

inherent absorption in the laser wavelength. However, based on the results presented herein, it is expected that with the blending of only several wt.% "carrier gas" sensitizers, the laser ablation efficiency and resolution for polymeric materials that are transparent at the laser wavelength could be greatly enhanced. While these new sensitizers have been initially explored in photopolymerized films, this sensitizer approach opens up the possibility of high precision laser microfabrication of a variety of polymer materials with a variety of properties.

4. Conclusions

A series of novel "carrier gas" laser ablation sensitizers were designed and synthesized by utilizing naphthalene as the UV laser energy absorber and the oxalyl group as the carrier gas generator. These sensitizers were then characterized by GC-MS, HPLC, FTIR and UV–vis. The synthesis and purification of OXT-DMO was difficult though enhanced laser ablation of a cationic UV curable coating was observed. The hydroxyl–acid chloride chemistry provided a facile, high yield route for the synthesis and purification of "carrier gas" sensitizers. Sensitizers were added into a masterbase formulation with the ratio of 0.0001 mol/5 g masterbase to formulate different sensitized coatings. Compared to the control sample, the sensitized coatings had no deterred UV curing and no significant change of thermal stability as revealed by RTIR and TGA, respectively, while optical profilometry and SEM revealed that all the sensitized coating samples were much better ablated than the control in 355 nm laser ablation experiments. Furthermore, it was shown that the addition of naphthalene or oxalyl modified polyols alone did not greatly enhance the material removal during UV laser ablation either due to the thermal effect or lack of absorption of the laser energy. On the other hand, the combination of both naphthalene and oxalyl groups, either blended or preferably, chemically bonded, showed a synergistic effect that results in much deeper, larger and cleaner ablated vias. One particular sensitizer, Na-MOC, with naphthalene and oxalyl group bound directly in one molecule, is especially effective considering its low addition level (<0.5 wt.%) and the resultant laser ablation enhancement. This result can be accounted for by Na-MOC's extended UV absorption and more efficient intramolecular utilization of the absorbed laser energy to generate carrier gases.

Acknowledgments

We would like to thank Prof. Orven Swenson in Physics Department of NDSU for the help in laser ablation experiments, Scott Payne for help with the Scanning Electron Microscopy experiments and David Christianson and Shane Stafslien of CNSE for assistance with GC-MS and HPLC experiments. This material is based on research sponsored by the Defense Microelectronics Activity (DMEA) under Agreements Numbers H94003-04-2-0406, and H94003-06-2-0601. The United States Government is authorized to reproduce and distribute reprints for Government purposes notwithstanding any copyright notation thereon.

References

[1] D.L. Pugmire, E.A. Waddell, R. Haasch, M.J. Tarlov, L.E. Locascio, Anal. Chem. 74 (2002) 871–878.
[2] T.S. Kunz, J. Stebani, J. Ihlemann, A. Wokaun, Appl. Phys. A 67 (1998) 347–352.
[3] T. Lippert, M. Hauer, C.R. Phipps, A. Wokaun, Appl. Phys. A 77 (2003) 259–264.
[4] T. Lippert, Adv. Polym. Sci. 168 (2004) 51–246.
[5] J.K. Kruger, W. Kautek, Adv. Polym. Sci. 168 (2004) 247–289.
[6] J.K. Kruger, W. Kautek, Appl. Surf. Sci. 96–98 (1996) 430–438.
[7] A.A. Serafetinides, M.I. Makropoulou, C.D. Skordoulis, A.K. Kar, Appl. Surf. Sci. 180 (2001) 42–56.
[8] O. Nuyken, U. Dahn, A. Wokaun, T. Kunz, C. Hahn, V. Hessel, J. Landsiedel, Acta Polym. 49 (1998) 427–432.
[9] J.V. Koleske, O.K. Spurr, N.J. McCarthy, Nation. SAMPE Techn. Conf. 14 (1982) 249–256.
[10] J.V. Koleske, N.J. McCarthy, O.K. Spurr, Nation. SAMPE Techn. Conf. 16 (1984) 529–536.
[11] J.X. Chen, M.D. Soucek, J. Coat. Technol. 75 (2003) 49–58.
[12] Z. Chen, D.C. Webster, Polymer 47 (2006) 3715–3726.
[13] M.C. Jang, J.V. Crivello, J. Polym. Sci.: Part A: Polym. Chem. 41 (2003) 3056–3073.
[14] T. Lippert, J.T. Dickinson, Chem. Rev. 103 (2003) 453–485.
[15] H. Fukumura, H. Masuhara, Chem. Phys. Lett. 221 (1994) 373–378.
[16] G.B.J. Blanchet, J. Appl. Phys. 80 (1996) 4082–4089.
[17] Z. Chen, D.C. Webster, J. Polym. Sci.: Part A: Polym. Chem. 44 (2006) 4435–4449.
[18] J.V. Crivello, F. Jiang, Chem. Mater. 14 (2002) 4858–4866.
[19] E.W. Nelson, T.P. Carter, A.B. Scranton, Polym. Mater. Sci. Eng. 69 (1993) 363–364.
[20] J.D. Cho, H.K. Kim, Y.S. Kim, J.W. Hong, Polym. Test. 22 (2003) 633–645.
[21] Y. Hua, F. Jiang, J.V. Crivello, Chem. Mater. 14 (2002) 2369–2377.